Changes in Zonal Surface Temperature Gradients and Walker Circulations in a Wide Range of Climates

TIMOTHY M. MERLIS AND TAPIO SCHNEIDER

California Institute of Technology, Pasadena, California

ABSTRACT

Variations in zonal surface temperature gradients and zonally asymmetric tropical overturning circulations (Walker circulations) are examined over a wide range of climates simulated with an idealized atmospheric general circulation model (GCM). The asymmetry in the tropical climate is generated by an imposed ocean energy flux, which does not vary with climate. The range of climates is simulated by modifying the optical thickness of an idealized longwave absorber (representing greenhouse gases).

The zonal surface temperature gradient in low latitudes generally decreases as the climate warms in the idealized GCM simulations. A scaling relationship based on a two-term balance in the surface energy budget accounts for the changes in the zonally asymmetric component of the GCM-simulated surface temperature.

The Walker circulation weakens as the climate warms in the idealized simulations, as it does in comprehensive simulations of climate change. The wide range of climates allows a systematic test of energetic arguments that have been proposed to account for these changes in the tropical circulation. The analysis shows that a scaling estimate based on changes in the hydrological cycle (precipitation rate and saturation specific humidity) accounts for the simulated changes in the Walker circulation. However, it must be evaluated locally, with local precipitation rates. If global-mean quantities are used, the scaling estimate does not generally account for changes in the Walker circulation, and the extent to which it does is the result of compensating errors in changes in precipitation and saturation specific humidity that enter the scaling estimate.

1. Introduction

The evolution of zonal surface temperature gradients in the tropics is of interest in the study of future and past climates (e.g., Knutson and Manabe 1995; Fedorov et al. 2006). Recently, the changes in the zonally asymmetric component of the tropical overturning circulation, the Walker circulation, have been highlighted as a robust response to warming in climate change simulations with comprehensive GCMs (Held and Soden 2006; Vecchi and Soden 2007). Here, we examine the response of these zonally asymmetric aspects of the mean tropical climate to radiative perturbations in an idealized GCM and test theoretical arguments designed to account for their changes.

How zonal surface temperature gradients evolve as the climate warms is unclear. On one hand, increased cooling associated with the upwelling of cold water on the eastern ocean margins may lead to increased zonal temperature gradients in transient warmings (Clement et al. 1996), and this mechanism appears to be important in coupled GCM simulations (Held et al. 2010). On the other hand, paleoclimate evidence from the Pliocene suggests substantially weakened or collapsed zonal temperature gradients in a climate only somewhat warmer than Earth's current climate (e.g., Fedorov et al. 2006). [However, see Wunsch (2009) for an alternative interpretation of the data.] The multimodel mean of the fourth Intergovernmental Panel on Climate Change (IPCC) assessment models shows little change in zonal temperature gradients in the Pacific basin over the twenty-first century (DiNezio et al. 2009). As a step toward understanding the full climate dynamics that control the zonal surface temperature gradient in the tropics, we develop a scaling relationship based on the surface energy budget and compare it to the results of the idealized GCM simulations.

The connection between changes in the hydrological cycle and large-scale atmospheric circulations in response

Corresponding author address: Timothy M. Merlis, California Institute of Technology, 1200 California Blvd., MC 100-23, Pasadena, CA 91125.
E-mail: tmerlis@caltech.edu

to radiative forcing, for instance, by changed greenhouse gas concentrations, can be subtle. For example, the mass fluxes in the Hadley cell and extratropical eddy kinetic energy can vary nonmonotonically as a longwave absorber is systematically varied in an idealized GCM, with implications for water vapor fluxes and the distribution of evaporation and precipitation (O'Gorman and Schneider 2008a,b; Schneider et al. 2010; Levine and Schneider 2011).

Analysis of comprehensive GCM simulations suggests the connection between changes in the hydrological cycle and upward mass fluxes is straightforward (Held and Soden 2006; Vecchi and Soden 2007). The argument is that precipitation, which is constrained by the energy balance at the surface in the global mean, increases with warming more slowly than near-surface specific humidity, which increases similarly to the rate given by the Clausius–Clapeyron relation for small changes in relative humidity; thus, the upward vertical velocity that gives rise to condensation of water vapor weakens. This scaling argument is sometimes interpreted to account for changes in the Walker circulation (e.g., Vecchi et al. 2006), in part because changes in the zonally asymmetric component of the circulation are larger than those in the zonally symmetric component (Held and Soden 2006). A difficulty in applying the hydrological cycle argument directly to local circulations, such as the Walker circulation, is that the surface energy balance constraint on the precipitation is lost, as water vapor convergence depends locally on the atmospheric circulation. A central goal of this work is to assess the extent to which the hydrological cycle arguments apply locally to the Walker circulation, and to compare this to global-mean versions of the scaling arguments to determine the extent to which they are adequate.

Here, we use an idealized GCM to systematically examine the response of the zonally asymmetric tropical surface temperature and the Walker circulation to changes in the atmosphere longwave opacity. A scaling estimate based on the surface energy balance accounts for the changes in the zonal surface temperature gradient. We assess the hydrological cycle estimate for changes in the Walker circulation by applying it locally. The scaling estimate is accurate, though it requires knowledge of the precipitation field. In contrast, the global-mean version of the scaling estimate does not in general account for the Walker circulation changes.

2. Idealized GCM

a. Model description

We use an idealized, moist primitive-equation atmospheric GCM similar to those described in O'Gorman and Schneider (2008b) and Frierson et al. (2006). Briefly, the model includes an active hydrological cycle with a simplified Betts–Miller convection scheme (Frierson 2007). The scheme relaxes over a fixed time scale convectively unstable columns to moist pseudoadiabatic temperatures with constant (70%) relative humidity. It has a gray longwave radiation scheme, and a slab-ocean surface boundary condition with the heat capacity of 1 m of water. The top-of-atmosphere insolation is an idealized, annual-mean profile, and there is shortwave absorption in the atmosphere, both of which are as described in O'Gorman and Schneider (2008b). There is no condensed water phase in the atmosphere (i.e., there are no clouds). The climate is perturbed by varying the optical depth in the gray radiation scheme by a multiplicative factor to mimic variations in the trapping of longwave radiation due to variations in greenhouse gas concentrations. The primitive equations are integrated using the spectral transform method in the horizontal with T85 resolution (but the simulation results are similar with T42 resolution). Finite differences in $\sigma = p/p_s$ (with pressure p and surface pressure p_s) discretize the vertical coordinate, with 30 unevenly spaced levels. The time stepping is semi-implicit, with a leapfrog time step of 300 s. The simulation statistics are averaged over the last 1100 days of the simulation following a spinup period of either 700 days for an isothermal, resting initial condition or 300 days for an initial condition from an equilibrated simulation with similar optical thickness. Aside from the horizontal resolution and time step, the only difference between the simulations presented here and those presented in O'Gorman and Schneider (2008b) is that we include a representation of ocean energy flux divergence in the slab ocean and present fewer simulated climates.

b. Prescribed ocean energy flux divergence

The surface boundary condition is a slab ocean that accounts for the radiative and turbulent surface fluxes. Additionally, it has a prescribed ocean energy flux divergence that represents the influence of the ocean circulation on the surface temperature. This is commonly referred to as a Q-flux in climate modeling.

The Q-flux consists of a component that varies only in latitude and represents the divergence of the meridional ocean energy flux

$$\nabla \cdot F_0(\phi) = Q_0\left(\frac{1 - 2\phi^2}{\phi_0^2}\right)\exp\left(-\frac{\phi^2}{\phi_0^2}\right), \qquad (1)$$

where ϕ is latitude, $\phi_0 = 16°$, and $Q_0 = 50$ W m^{-2} following Bordoni (2007) and Bordoni and Schneider (2008). The meridional component of the Q-flux is necessary to have an Earth-like tropical circulation in the reference climate; without it, the zonal-mean (Hadley)
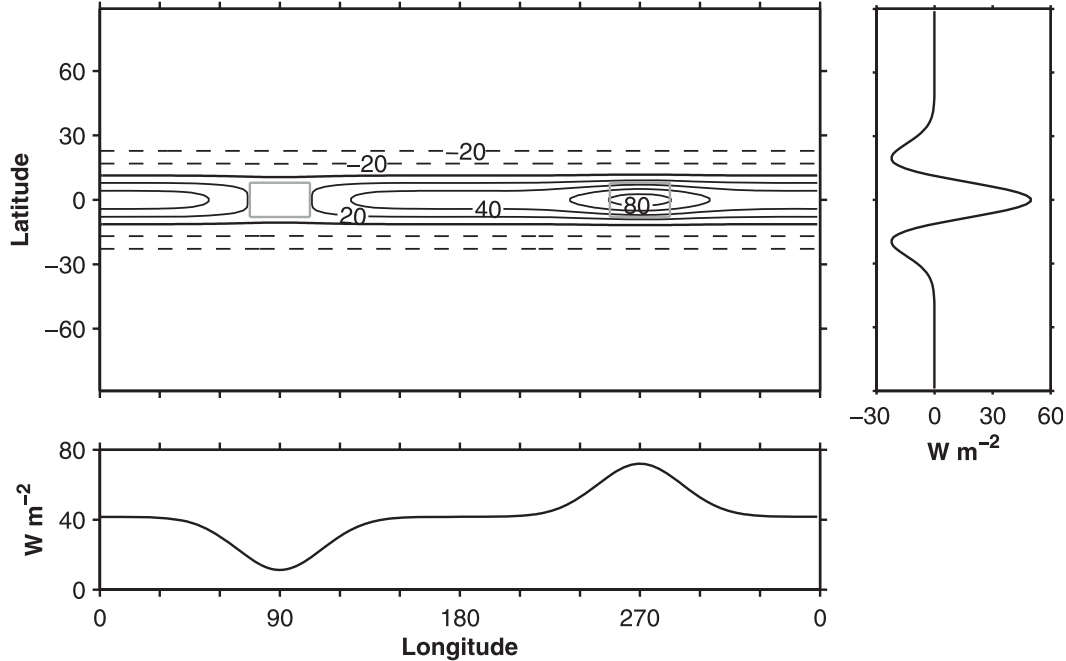
FIG. 1. Ocean energy flux divergence, Q-flux, for which positive values indicate cooling tendencies. (top left) Longitude–latitude Q-flux contours with contour interval of 20 W m^{-2}, and negative values are dashed. The gray rectangles indicate the averaging regions. (right) Latitude vs zonal-mean Q-flux and (bottom) equatorial Q-flux (averaged within 8° of the equator) vs longitude.

circulation is sufficiently strong that there is mean ascending motion everywhere along the equator (i.e., the descending branch of the Walker circulation is weaker than the Hadley circulation).

Zonal symmetry is broken by adding and subtracting Gaussian lobes along the equator that are spaced 180° longitude apart,

$$\nabla \cdot [F_0(\phi) + F_1(\lambda, \phi)] = \nabla \cdot F_0(\phi)$$
$$+ Q_1 \exp\left[-\frac{(\lambda - \lambda_E)^2}{\lambda_1^2} - \frac{\phi^2}{\phi_1}\right]$$
$$- Q_1 \exp\left[-\frac{(\lambda - \lambda_W)^2}{\lambda_1^2} - \frac{\phi^2}{\phi_1}\right], \quad (2)$$

where λ is longitude, $\lambda_1 = 30°$, $\lambda_E = 90°$, $\lambda_W = 270°$, $\phi_1 = 7°$, and $Q_1 = 40$ W m^{-2}.

The resulting Q-flux, shown in Fig. 1, has similar magnitude and spatial scale to reanalysis estimates (e.g., Trenberth et al. 2001, their Fig. 5).

c. Series of simulations

As in O'Gorman and Schneider (2008b), the longwave optical depth is varied to mimic changes in greenhouse gas concentrations. The optical depth $\tau = \alpha \tau_{ref}$ is the product of a multiplicative factor α and a reference profile τ_{ref} that depends on latitude and pressure,

$$\tau_{ref} = [f_l \sigma + (1 - f_l)\sigma^4][\tau_{eq} + (\tau_p - \tau_{eq}) \sin^2\phi], \quad (3)$$

where $f_l = 0.2$ and the reference optical depths at the equator and pole are $\tau_{eq} = 7.2$ and $\tau_p = 1.8$, respectively. We conduct simulations with rescaling factors $\alpha = (0.6, 0.7, 0.8, 0.9, 1.0, 1.2, 1.4, 1.6, 1.8, 2.0, 2.5, 3.0, 4.0, 6.0)$. The range of optical depths presented here is reduced compared to O'Gorman and Schneider (2008b); simulations with the smallest optical depths are omitted because the fixed meridional Q-flux leads to reversed Hadley cells and concomitant double intertropical convergence zones in sufficiently cold climates. In total, 14 simulations are presented here.

3. Zonal surface temperature gradients

a. Simulation results

Figure 2 shows the simulated zonal surface temperature differences averaged over the regions indicated in Fig. 1 for each of the equilibrated climates, which are identified by the time- and global-mean (denoted $\langle \cdot \rangle$) surface temperature $\langle T_s \rangle$. Following O'Gorman and Schneider (2008b), the reference climate with $\alpha = 1.0$ is indicated by a filled symbol. The east–west surface temperature difference ΔT_s decreases nearly monotonically as the climate warms and varies by more than a factor of 3 over the simulated range of climates.
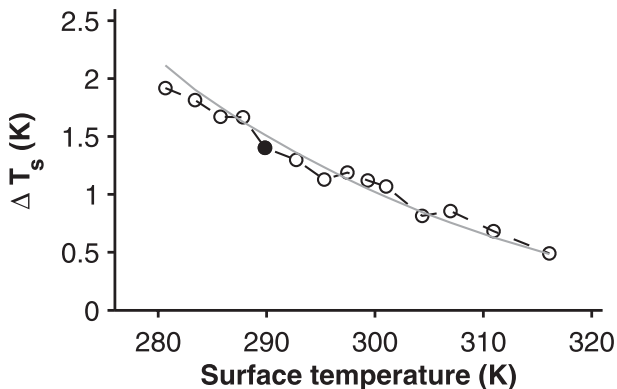
FIG. 2. Zonal surface temperature difference (west minus east in Fig. 1) vs global-mean surface temperature of GCM simulations (circles with black dashed line), and scaling estimate (8) (gray line). The averaging conventions used to evaluate the scaling estimate are described in the text.

The simulated zonal temperature difference in the reference climate (1.4 K) is smaller than that in Earth's current climate (~5 K). While we have used a Q-flux that has comparable magnitude to estimates for the current climate, the lack of clouds, and the concomitant zonal asymmetry in cloud radiative forcing leads to a smaller zonal asymmetry in the equilibrated surface temperature. One remedy would be to impose a larger asymmetry in the Q-flux since in quasi-equilibrium theory there is a near equivalence between surface fluxes and radiative

forcing (Sobel et al. 2010, section 2.3). However, we chose not to amplify the Q-flux asymmetry. Therefore, it is more meaningful to consider fractional changes in the simulated zonal surface temperature contrast than the magnitude of the simulated changes. Our results hence may give changes in the surface temperature contrasts that, in reality, would likely be modified by processes we ignored, such as cloud–radiative feedbacks.

b. Scaling estimate

Figure 3 shows the surface energy budget as a function of longitude for the Earth-like reference simulation. Examining the variations in longitude of the surface energy balance reveals that the dominant balance in the zonally asymmetric component is between the prescribed Q-flux and the evaporative fluxes. This is to be expected in Earth-like and warmer climates where the Bowen ratio (ratio of sensible to latent surface fluxes) is small in the tropics. An analogous ratio can be formed for the net longwave radiation at the surface (Pierrehumbert 2010), and this is also small for sufficiently warm climates.

This two-term balance between the zonally asymmetric component of the Q-flux $\nabla \cdot F_1$ and evaporation holds over the range of climates we simulate, so that

$$\Delta(\nabla \cdot F_1) \sim \Delta \mathrm{LE}, \qquad (4)$$
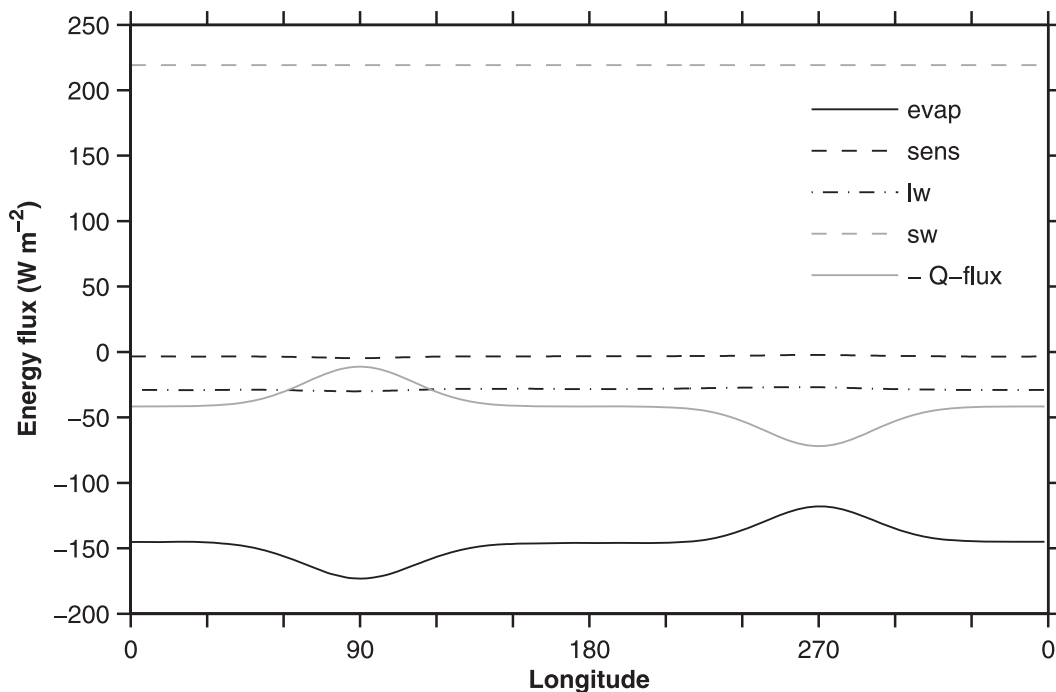
where Δ refers to east–west differences.

FIG. 3. Surface energy fluxes of the reference simulation vs longitude averaged within 8° of equator. Here, "lw" and "sw" refer to the net longwave and shortwave radiative fluxes at the surface, respectively.

As the Q-flux is fixed, the bulk aerodynamic formula for evaporative fluxes can be manipulated with suitable assumptions to invert the zonal difference in the evaporative fluxes into a zonal difference in the surface temperature. The evaporative fluxes are computed by the bulk aerodynamic formula

$$E = \rho c_d \|\mathbf{v}\|[q_s(T_s) - q] \approx \rho c_d \|\mathbf{v}\|(1 - \mathcal{H})q_s(T_s), \quad (5)$$

with air density ρ, drag coefficient c_d, surface wind speed $\|\mathbf{v}\|$, saturation specific humidity q_s, specific humidity of surface air q, surface temperature T_s, and surface relative humidity $\mathcal{H}$. The second formula is approximate in that the ratio of the specific humidity and the saturation specific humidity is set equal to the relative humidity and in that the air–sea temperature difference is neglected. Neglecting the air–sea temperature difference is justifiable because the subsaturation of air dominates over the air–sea temperature difference for conditions typical of tropical oceans.

For the climate changes we are examining, the east–west evaporation difference then scales like the east–west difference in the surface saturation specific humidity[1]

$$\Delta E \sim \Delta q_s(T_s). \quad (6)$$

This is the result of the strong dependence of q_s on temperature (fractional changes of approximately 7% K^{-1} for Earth-like temperatures). In contrast, changes in $\mathcal{H}$ are relatively small. For example, Schneider et al. (2010) presented an argument based on a simplified surface energy budget that suggests approximately 1% K^{-1} changes in $\mathcal{H}$. Regional changes that affect the zonal gradient of relative humidity are potentially important, but neither comprehensive GCM simulations (O'Gorman and Muller 2010) nor the idealized GCM simulations presented here exhibit substantial changes in the zonal relative humidity gradient. The neglected changes in the air–sea temperature difference and surface wind speed are also generally smaller than the changes in the surface saturation specific humidity.

To obtain an east–west surface temperature difference, rather than a saturation specific humidity difference, we linearize the saturation specific humidity

$$\Delta q_s(T_s) \approx \frac{\partial q_s}{\partial T} \Delta T_s. \quad (7)$$

The resulting scaling estimate for the east–west temperature difference is the product of the east–west saturation specific humidity difference Δq_s and the inverse of the rate of change of the saturation specific humidity with temperature:

$$\Delta T_s \sim \Delta q_s \left(\frac{\partial q_s}{\partial T}\right)^{-1}. \quad (8)$$

For invariant ocean energy fluxes, as in the idealized GCM simulations, Δq_s is approximately constant by Eqs. (4) and (6), and the east–west surface temperature difference will decrease with warming by an amount given by the rate of change of the saturation specific humidity with temperature (i.e., given by the Clausius–Clapeyron relation as the surface pressure is nearly constant), evaluated using a temperature that is representative of the surface in the tropics.

The decrease in the zonal temperature difference in a warming scenario can be anticipated by considering the counterexample of invariant zonal surface temperature gradients: if the east–west temperature difference remained the same as the mean climate warmed, in the absence of changes in near-surface relative humidity, the east–west difference in evaporative fluxes would rapidly increase with warming. The resulting zonal asymmetry in the evaporation would be too large to be balanced by an invariant ocean energy flux, and the other terms in the surface energy balance are too small to restore equilibrium. In a transient adjustment, the excess in evaporation would lead to a reduction in the east–west surface temperature asymmetry as, for example, the large evaporation over warm regions would cool the surface. The sensitivity of the evaporative fluxes to climate change and concomitant reduction in zonal surface temperature gradients with warming was documented in the GCM simulations of Knutson and Manabe (1995), who called it "evaporative damping."

These approximations are adequate for the longwave radiation–induced climate changes in the idealized GCM simulations, though they may not be in general. For example, in analyses of climate change simulations, Xie et al. (2010) showed that changes in surface winds must be accounted for in the surface energy budget of some regions, and DiNezio et al. (2009) showed that cloud–radiative feedbacks affect the net surface shortwave radiation.

c. Assessment of scaling estimate

Figure 2 shows the scaling estimate (8) in gray. The derivative of the saturation specific humidity with respect to temperature in Eq. (8) is evaluated with the same simplified formulation for the saturation specific

---

[1] We are not suggesting that this scaling holds in general [see, e.g., O'Gorman and Schneider (2008b) and our Fig. 6 for a counterexample in the global mean] but only for the zonal difference in the tropics.

humidity as is used in the GCM, using the simulated time- and zonal-mean surface temperature averaged within 8° of latitude of the equator. Evaluated over the averaging regions in Fig. 1, Δq_s varies by approximately 15% over the range of simulations, and we use the mean value, 2.4×10^{-3}, in the scaling estimate. The magnitude of the variations in Δq_s is consistent with the magnitude of the neglected terms in the bulk aerodynamic formula. Overall, there is close agreement (maximum deviations $\approx$ 15%) between the scaling estimate and the results of the GCM simulations.

We note that while the simulations and scaling estimate feature rapidly decreasing zonal temperature gradients as the mean temperature increases (7.4% K^{-1} at the reference climate), the decreases are not as rapid as proxies of the Pliocene suggest ($\sim$15%–30% K^{-1}). But it is possible that the neglected radiative and ocean feedbacks increase the sensitivity to changes.

4. Walker circulation

a. Simulation results

Figure 4 shows the zonally asymmetric component of the time-mean pressure velocity, $Dp/Dt = \omega$, in the longitude–sigma plane for three simulations.[2] The zonally asymmetric pressure velocity is large over the regions of perturbed Q-flux; it is small elsewhere. The pressure depth over which it has large amplitude increases with warming because the tropopause height increases; its magnitude decreases with warming. Note that a consequence of the Walker circulation's localization over the Q-flux perturbations is that the averaging convention we have chosen is adequate to capture nearly all of the ascending and descending mass fluxes—it is a closed circulation and alternative measures, such as surface pressure differences, yield similar results.

Figure 5 shows that the Walker circulation mass flux in the ascending region rapidly weakens with warming. The fractional rate of decrease is 4.4% K^{-1} at the reference climate relative to the global-mean surface temperature. (The fractional change is larger relative to local surface temperature changes as the warming is greater in high latitudes.) The Walker circulation varies by a factor of 6 over the simulated range of climates. In this figure, the zonally asymmetric component of the pressure velocity is evaluated on the sigma surface where it is maximum, which varies from $\sigma = 0.60$ in the coldest climate to $\sigma = 0.32$ in the warmest climate.
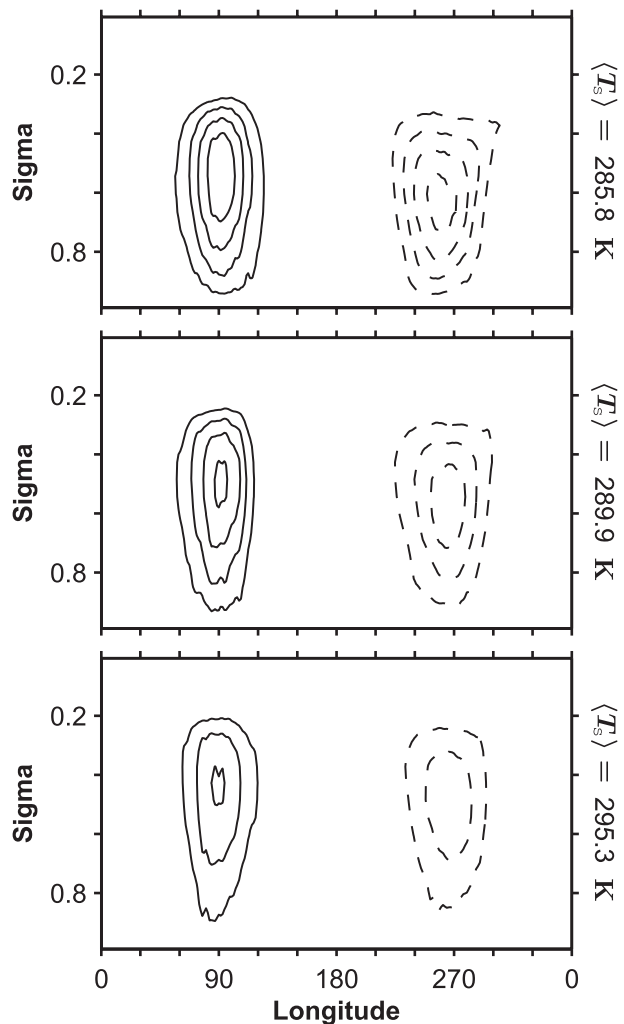
---

[2] All figures show $p_s D\sigma/Dt$, which differs only slightly ($\sim$0.1% in the region of interest) from Dp/Dt as $\sigma Dp_s/Dt$ is small.

FIG. 4. Contours of the zonally asymmetric component of the time-mean pressure velocity $\overline{\omega}^*$ in the longitude–sigma plane averaged within 8° of the equator for three simulations with global-mean surface temperature $\langle T_s \rangle$ indicated on the right. The contour interval is 0.01 Pa s^{-1} with positive values (descending motion) dashed. The zero contour is omitted.

These changes roughly follow those of the zonal-mean tropical tropopause (averaged within 8° of the equator), which rises from $\sigma = 0.24$ to $\sigma = 0.03$ determined by the World Meteorological Organization (WMO) 2 K km^{-1} lapse rate criterion. If the Walker circulation is evaluated using fixed sigma levels in the lower troposphere, the weakening with warming is more rapid owing to the combined changes in the vertical structure of the circulation and the changes, shown in Fig. 5, that are independent of the vertical structure.

b. Scaling estimate

In saturated ascending motion, the vertical advection of saturation specific humidity q_s leads to condensation c,
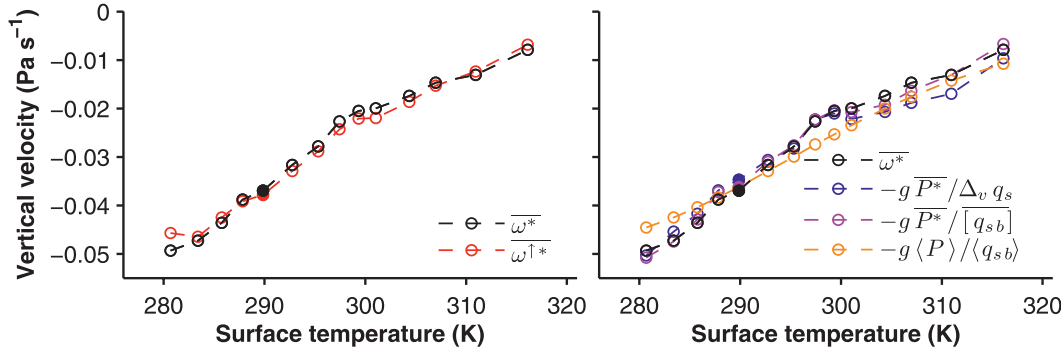
FIG. 5. (left) Zonally asymmetric component of the pressure velocity $\overline{\omega^*}$ (black) and zonally asymmetric component of the upward pressure velocity $\overline{\omega^{\uparrow*}}$ (red) averaged over the ascending region of the Walker circulation (cf. Fig. 1) vs global-mean surface temperature. Here, $\overline{\omega^*}$ is evaluated on the sigma level where it is minimum (strongest ascent), and $\overline{\omega^{\uparrow*}}$ is evaluated on the same level. The upward velocity has been multiplied by a factor of 1.3 determined by minimizing the mean squared deviation between $\overline{\omega^{\uparrow*}}$ and $\overline{\omega^*}$. (right) The $\overline{\omega^*}$ (black) and hydrological cycle scaling estimates: $-g\,\overline{P^*}/\Delta_v q_s$ (blue), $-g\,\overline{P^*}/\overline{[q_{sb}]}$ (magenta), and $-g\langle P\rangle/\langle q_{sb}\rangle$ (orange). The scaling estimates are multiplied by constants of 1.5, 1.7, and 0.8, respectively, chosen to minimize the mean squared deviations between the scaling estimates and $\overline{\omega^*}$. The near-surface saturation specific humidity is evaluated on a fixed sigma level $\sigma = 0.96$. The free-tropospheric contribution to $\Delta_v q_s$ is evaluated on a sigma level that is a fixed amount larger than the sigma level of the tropopause, σ_t: $\sigma = \sigma_t + 0.15$. The scale estimates $\overline{P^*}/\Delta_v q_s$ and $\overline{P^*}/\overline{[q_{sb}]}$ are evaluated within 8° of the equator and $\langle P\rangle/\langle q_{sb}\rangle$ is evaluated using global means. Zonal averages are used for $\Delta_v q_s$ and $\overline{[q_{sb}]}$.

$$-\omega^{\uparrow}\partial_p q_s \approx c, \qquad (9)$$

where $\omega^{\uparrow} = \omega H(-\omega)$ is a truncated upward pressure velocity, and H is the Heaviside step function (Schneider et al. 2010). For a mass-weighted vertical average taken from the lifting condensation level to the tropopause (denoted by $\{\cdot\}$), the precipitation P balances the vertical advection of specific humidity:

$$-\{\omega^{\uparrow}\partial_p q_s\} \approx P. \qquad (10)$$

Equation (10) assumes that we are averaging over horizontal scales that are large enough to include convective downdrafts and the associated evaporation of condensate. Neglecting transients aside from those implicitly included by using the truncated vertical velocity, Eq. (10) can be decomposed into zonal-means, denoted by $[\cdot]$, and deviations thereof, denoted by an asterisk. The time mean, denoted by an overbar, of the zonally asymmetric component of the budget is then

$$-\{\overline{\omega^{\uparrow*}}\,\partial_p\overline{[q_s]} + \overline{[\omega^{\uparrow}]}\partial_p\overline{q_s^*} + \overline{\omega^{\uparrow*}}\partial_p\overline{q_s^*}$$
$$- \overline{[\omega^{\uparrow*}\partial_p q_s^*]}\} \approx \overline{P^*}. \qquad (11)$$

Terms 2–4 on the left-hand side, which include zonal asymmetries in saturation specific humidity $\overline{q_s^*}$, are negligible as a result of the weak temperature gradients in the free troposphere of the tropics (Charney 1963; Sobel et al. 2001). In the simulations, these terms combined are

an order of magnitude smaller than the terms in the dominant balance

$$-\{\overline{\omega^{\uparrow*}}\partial_p\overline{[q_s]}\} \approx \overline{P^*}. \qquad (12)$$

Our interest is in the zonally asymmetric component of the tropical overturning circulation (denoted $\overline{\omega^*}$), the Walker circulation, and so we estimate the mass fluxes of the ascending or descending branches from Eq. (12) as

$$-\frac{\overline{\omega^*}}{g} \sim -\frac{\overline{\omega^{\uparrow*}}}{g} \sim \frac{\overline{P^*}}{\Delta_v q_s}, \qquad (13)$$

where $\Delta_v q_s$ is a zonal-mean vertical saturation specific humidity difference.

This is closely related to the thermodynamic budget in the tropics where the stratification is close to moist adiabatic. On a moist adiabat (at constant saturation equivalent potential temperature θ_e^*), the vertical gradients of potential temperature θ and saturation specific humidity (assuming constant latent heat of vaporization) are related by

$$-(T/\theta)\partial_p\theta\Big|_{\theta_e^*} \approx (L/c_p)\partial_p q_s\Big|_{\theta_e^*} \qquad (14)$$

(e.g., Iribarne and Godson 1981). Thus, as discussed in Held and Soden (2006) and Schneider et al. (2010), the water vapor budget and thermodynamic budget are closely

linked. The zonally asymmetric component of both budgets is an approximate two-term balance between vertical advection of the zonal-mean potential temperature or saturation specific humidity by the zonally asymmetric velocity and the zonally asymmetric precipitation.

Held and Soden (2006) suggested that the free-tropospheric saturation specific humidity in scaling estimates for the upward mass flux is negligible or, as in Betts and Ridgway (1989) and Betts (1998), it is linearly related to the boundary layer saturation specific humidity $\overline{[q_{sb}]}$. In Eq. (13), $\Delta_v q_s \sim \overline{[q_{sb}]}$ leads to the scaling estimate

$$-\frac{\overline{\omega^*}}{g} \sim -\frac{\overline{\omega^{\uparrow *}}}{g} \sim \frac{\overline{P^*}}{\overline{[q_{sb}]}}. \tag{15}$$

Schneider et al. (2010) argued that the free-tropospheric contribution is not generally negligible—that is, an actual difference in saturation specific humidity must be considered in Eq. (13). Physically, this can occur as the result of the amplification of warming aloft for moist adiabatic stratification. However, the amplification of temperature increases at fixed pressure levels can be offset by increases in the pressure depth of the mass fluxes, as occur with a rising tropopause. A concrete example of offsetting changes in stratification and pressure depth is given by the "Fixed Anvil Temperature" hypothesis (Hartmann and Larson 2002), which posits that the temperature that convection reaches is approximately climate invariant. If this hypothesis holds precisely, the free-tropospheric saturation specific humidity at the tropical tropopause would also be climate invariant. Schneider et al. (2010) also showed that a scaling that includes the free-tropospheric contribution to the saturation specific humidity difference accounted better for changes in the upward component of zonal-mean tropical circulation in simulations with zonally symmetric forcing and boundary conditions.

Whether the free-tropospheric water vapor contributes depends on the vertical velocity profile $\Omega(p)$ that is used to separate the integrand: $\{\omega^{\uparrow} \partial_p q_s\} \approx \hat{\omega}^{\uparrow} \{\Omega(p)\partial_p q_s\}$, where $\hat{\omega}^{\uparrow}$ depends on the horizontal, but not the vertical, coordinates (e.g., Sobel 2007). This is discussed further in the appendix.

c. Assessment of scaling estimate

The left panel of Fig. 5 shows that the zonally asymmetric component of the pressure velocity in the ascent region scales with the zonally asymmetric component of the upward pressure velocity: $\overline{\omega^*} \sim \overline{\omega^{\uparrow *}}$. However, the zonally asymmetric total pressure velocity $\overline{\omega^*}$ is systematically larger (by about 30%) than $\overline{\omega^{\uparrow *}}$. The zonal-mean

upward vertical velocity $\overline{[\omega^{\uparrow}]}$ is larger than the zonal-mean total vertical velocity $\overline{[\omega]}$; hence, when the zonal-mean is removed to form the zonally asymmetric component (e.g., $\overline{\omega^*} = \overline{\omega} - \overline{[\omega]}$), $\overline{\omega^*}$ is larger than $\overline{\omega^{\uparrow *}}$. The fact that $\overline{\omega^*} \sim \overline{\omega^{\uparrow *}}$ suggests that if the hydrological cycle scaling estimate accounts for the changes in the upward pressure velocity, to which it is more directly related [Eq. (10)], it will also account for the changes in the total pressure velocity, that is, the Walker circulation. However, consistent with the results of Schneider et al. (2010), the simulated changes in $\overline{[\omega]}$ in the ascending branch of the Hadley circulation are not straightforwardly related to the changes in the upward component of $\overline{[\omega^{\uparrow}]}$.

The right panel of Fig. 5 shows that the hydrological cycle estimate (13) applied locally accounts for the changes in the Walker circulation. There are two variants of the local scaling in the right panel of Fig. 5: one includes the free-tropospheric saturation specific humidity contribution to $\Delta_v q_s$ (blue) and one that neglects it $\Delta_v q_s \sim \overline{[q_{sb}]}$ (magenta). The two are largely indistinguishable and both account for the simulated changes in $\overline{\omega^*}$. The scaling that neglects the free-tropospheric saturation specific humidity is an approximation, so while it appears to be more accurate in the warm limit, this is the result of compensating errors. The scaling constants, obtained by least squares, are approximately 1.5, which is consistent with the factor of 1.3 that relates $\overline{\omega^{\uparrow *}}$ and $\overline{\omega^*}$.

Figure 5 also shows the global-mean scaling estimate, $-g\langle P\rangle/\langle q_{sb}\rangle$, in orange. This is similar to the convention used in the analysis of IPCC simulations in Held and Soden (2006) and Vecchi and Soden (2007), who further approximated the saturation specific humidity changes by linearizing its dependence on temperature about the present climate (i.e., $\delta\langle q_{sb}\rangle \approx 0.07 \times \delta\langle T_s\rangle$). The global-mean scaling captures the gross magnitude of the weakening but not the detail. It tends to underestimate the circulation changes for climates colder than the reference climate; at the reference climate, the global-mean scaling decreases by 1.3% K^{-1}, compared with $\overline{\omega^*}$ which decreases by 4.4% K^{-1}.

As the local scaling convention captures the variations in the Walker circulation with climate, we can decompose it to determine the relative contributions from the precipitation changes (Fig. 6, left) and the saturation specific humidity changes (Fig. 6, right panel). Two factors—approximately constant $\overline{P^*}$ and rapidly decreasing $\Delta_v q_s^{-1}$ or $\overline{[q_{sb}]}^{-1}$—account for the rapid decrease in the Walker circulation with warming.

The zonally asymmetric component of tropical precipitation $\overline{P^*}$ is approximately constant with climate; however, this is not a general result. Alternative convection scheme parameters, in particular relaxing to 90%
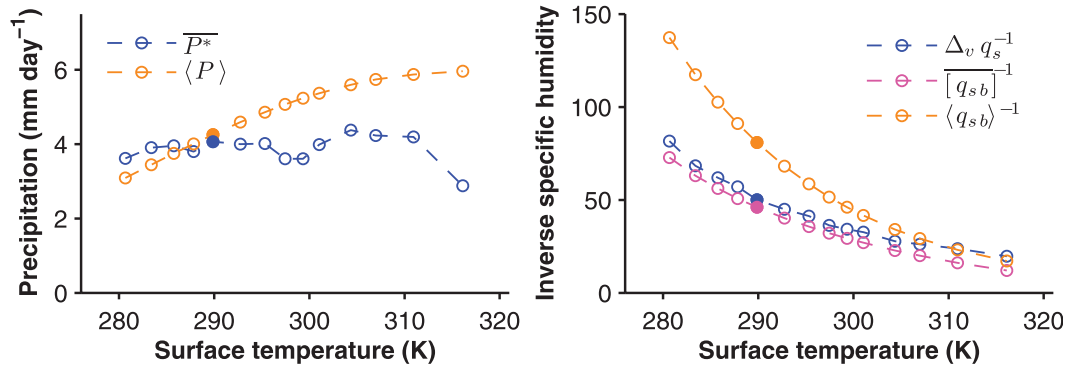
FIG. 6. (left) Precipitation vs global-mean surface temperature for zonally asymmetric tropical-mean $\overline{P^*}$ (blue) and global-mean $\langle P \rangle$ (orange). (right) Inverse specific humidity vs global-mean surface temperature for tropical-mean $\Delta_v q_s$ (blue), tropical-mean $\overline{[q_{sb}]}$ (magenta), and global-mean $\langle q_{sb} \rangle$ (orange). The averaging conventions are the same as in Fig. 5.

relative humidity instead of 70%, can produce non-monotonic changes in $\overline{P^*}$ with climate. The locally averaged version of the scaling for Walker circulation changes (13) is similarly accurate in the alternate set of simulations. These simulations have increases in $\overline{P^*}$ and a less rapid decrease in the Walker circulation $\overline{\omega^*}$ with warming from the Earth-like reference climate than the simulations presented here. The multimodel mean of the models participating in the fourth IPCC assessment also features increased $\overline{P^*}$ with warming (Meehl et al. 2007).

Changes in local precipitation cannot be understood independently of the circulation changes as local water vapor convergence depends, in part, on the circulation changes. In the simulations presented here, the changes in the zonally asymmetric component of net precipitation in the deep tropics have a large dynamic component, that is, a component associated with changed winds and fixed specific humidity. The dynamic changes reduce the zonally asymmetric precipitation due to weakening surface easterlies with warming and offset the thermodynamic component of the changes, that is, the component associated with changes in specific humidity and fixed winds, which increase the zonally asymmetric precipitation with warming. This is qualitatively consistent with the multimodel mean of the fourth IPCC assessment simulations presented in Fig. 7 of Held and Soden (2006): the equatorial Pacific is a region in which the changes in net precipitation are quite different from a thermodynamic estimate that assumes fixed circulation.

The saturation specific humidity is a rapidly increasing function of temperature, so, as expected, its inverse rapidly decreases with warming. The difference between the inverse saturation specific humidity when the free-tropospheric component of $\Delta_v q_s$ is neglected and when it is retained is small. This is a consequence of the depth of the circulation—it reaches sufficiently low pressures and

temperatures that q_s is negligible in that region of the free troposphere. The appendix has a more extensive discussion of the dependence of the scaling estimate on the vertical structure of the circulation and how the results of the simulations presented here relate to previous work.

Figure 6 also sheds light on why the global-mean convention may, in some cases, appear adequate. Global-mean precipitation $\langle P \rangle$ increases more rapidly than the zonally asymmetric component of tropical precipitation $\overline{P^*}$; global-mean surface saturation specific humidity $\langle q_{sb} \rangle$ increases more rapidly than the tropical-mean saturation specific humidity difference $\Delta_v q_s$. As the scaling depends on the ratio, the more rapid changes in the individual components largely cancel, but this must be regarded as fortuitous.

5. Conclusions

Zonal surface temperature gradients decrease rapidly as the climate warms in the idealized GCM. This can be understood by considering a simplified surface energy budget that consists of a two-term balance between the zonally asymmetric component of the Q-flux and evaporation. It leads to a scaling for the zonal difference in tropical surface temperature that depends inversely on the rate of change of saturation specific humidity (or the Clausius–Clapeyron relation), evaluated using the mean surface temperature in the tropics if the Q-flux is fixed.

The Walker circulation rapidly weakens with warming in the idealized GCM. The changes can be accounted for using locally evaluated hydrological cycle scaling estimates. The changes in the scalings can be decomposed into (i) equatorial precipitation increases being approximately zonally uniform with warming and (ii) rapid, Clausius–Clapeyron increases in near-surface saturation specific humidity with warming. The global-mean version of the hydrological cycle scale estimate does not accurately

account for the changes in the Walker circulation in all climates, though it does capture gross changes due to compensating changes in precipitation and saturation specific humidity that are larger than the locally averaged quantities.

That the hydrological cycle scaling estimate requires knowledge of local precipitation changes is a limitation. Ideally, one would want to understand circulation changes independently and use that result in the water vapor budget to constrain local precipitation changes. The moist static energy budget is one approach, though it has established difficulties (Sobel 2007). Another approach is that of the Lindzen–Nigam model (Lindzen and Nigam 1987), in which the surface temperature field is used to determine pressure gradients, which in combination with a linear momentum equation determine boundary layer convergence. We have solved the Lindzen–Nigam equations using the GCM-simulated surface temperature fields as forcing and found that the changes the Lindzen–Nigam model predicted in the boundary layer mass flux underestimated those simulated by the GCM by roughly a factor of 2 over the range of climates. Devising conceptual models of how tropical circulations change with climate that adequately account for GCM simulations remains a challenge.

A limitation of this study is the prescribed and invariant Q-flux. But understanding the atmosphere-only dynamics is a necessary step toward the more realistic case that includes an interactive ocean.

APPENDIX

Dependence of Water Vapor Scaling on Vertical Structure

To understand why the free-tropospheric contribution to the saturation specific humidity difference is negligible,
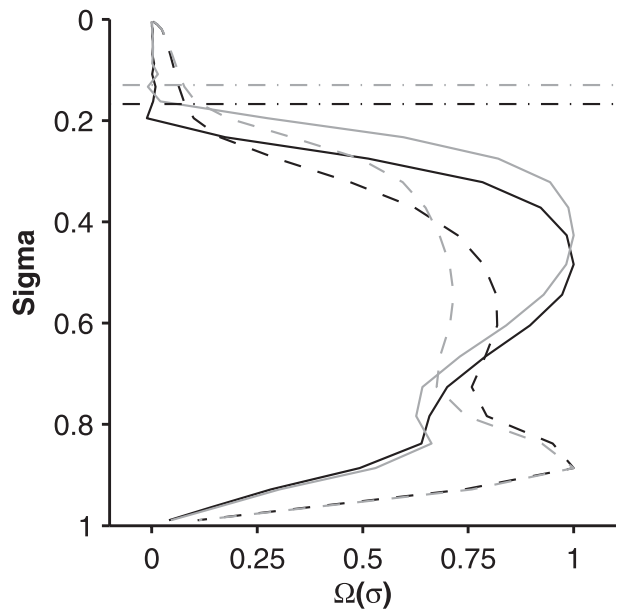

FIG. A1. Vertical structure of vertical velocity $\Omega(\sigma) = \omega^{\uparrow}/\min(\omega^{\uparrow})$ for simulations with $\langle T_s \rangle = 289.9$ K (black) and 295.3 K (gray). Solid lines are zonally asymmetric pressure velocity profiles $\overline{\Omega^*}$ evaluated in the ascending region (cf. Fig. 1) and dashed lines are zonal-mean pressure velocity profiles $[\overline{\Omega}]$. The dashed–dotted lines are the zonal-mean tropical tropopause defined by the WMO 2 K km^{-1} lapse rate criterion.

we examine the vertical structure of the vertical velocity, as $\Delta_v q_s$ is an approximation of $\{\Omega(p)\partial_p q_s\}$. Also, the vertical structure of the circulation has importance beyond the hydrological cycle scaling estimate: it determines whether moist static energy is imported or exported by overturning circulations (Sobel 2007; Back and Bretherton 2006; Peters et al. 2008). If the vertical velocity profile has larger amplitude in the free troposphere, it makes the saturation specific humidity difference less sensitive to the free-tropospheric values entering $\Delta_v q_s$ because temperature and saturation specific humidity are small there. Indeed, the vertical velocity profile is "top-heavy" in the ascending branch of the Walker circulation (solid lines in Fig. A1); that is, it has significant amplitude in the upper troposphere. In contrast, the zonal-mean vertical velocity profile has more amplitude near the surface and less amplitude in the upper troposphere (dashed lines in Fig. A1). The vertical velocity profiles of the idealized simulations are broadly consistent with the regional variations in the vertical velocity profile in Earth's tropics (Back and Bretherton 2006).

For the zonal-mean component of the simulations presented here, the hydrological cycle scaling estimate that neglects the changes in the saturation specific humidity away from the boundary layer ($\Delta_v q_s \sim [\overline{q_{sb}}]$) is distinguishable from the scaling estimate that retains the

full $\Delta_v q_s$ (i.e., the representative pressure levels when the integral is discretized are closer to each other than in the zonally asymmetric case and the free-tropospheric contribution is not negligible). This is consistent with the results presented in Schneider et al. (2010).

Figure A1 also shows that the pressure depth over which there is significant vertical velocity amplitude increases and the tropopause pressure decreases with warming. For this reason, we vary the pressure at which the free-tropospheric contribution to $\Delta_v q_s$ is evaluated in Fig. 5; neglecting these changes can potentially lead to different scaling behavior.

There are two ways in which the vertical velocity profile can lead to Clausius–Clapeyron-like scaling of $\Delta_v q_s$. First, a larger pressure depth decreases the free troposphere's weight (e.g., in the limit of the whole troposphere, the tropopause saturation specific humidity is orders of magnitude smaller than that of the surface). Second, holding the pressure depth fixed and shifting it upward (e.g., the difference between 800 and 300 hPa compared to the difference between 900 and 400 hPa) leads to more rapid changes in the saturation specific humidity difference as the temperatures are lower and the rate of change of the saturation specific humidity is larger. These changes will appear closer to the rate given by the Clausius–Clapeyron relation if it is evaluated at a fixed level such as the surface (related issues about the sensitivity of saturation specific humidity to where it is evaluated and the possible imprecision that results are discussed in O'Gorman and Muller 2010).

In an analysis of comprehensive GCMs, Vecchi and Soden (2007) showed that changes in the global-mean upward component of the vertical velocity scaled with the hydrological cycle scaling estimate that neglects the free-tropospheric contribution to the saturation specific humidity (i.e., $\langle \omega^\uparrow \rangle \sim -g\langle P \rangle / \langle q_{sb} \rangle$), but the scaling overestimated the magnitude of the vertical velocity changes by about a factor of 2–3. However, when Vecchi and Soden (2007) considered only upward pressure velocities exceeding 0.05 Pa s^{-1} [i.e., $\omega^\uparrow = \omega H(-0.05$ Pa s$^{-1} - \omega)$], the changes in the vertical velocity were larger and consistent with the scaling estimate. Changes in the vertical structure of the circulation may explain why the scaling in Fig. 5 of Vecchi and Soden (2007) improved when a nonzero threshold for upward vertical velocity was introduced: with a threshold of zero, the vertical velocity profile is less top heavy and the changes in the free-tropospheric saturation specific humidity contribution to $\Delta_v q_s$ cannot be neglected, in which case approximating $\Delta_v q_s$ with $\overline{q_{sb}}$ leads to an overestimate of the predicted weakening of the circulation with warming; however, for regions of strong ascent (such as those considered here), the vertical velocity profile can

be sufficiently deep that the free-tropospheric contribution to $\Delta_v q_s$ is negligible, $\Delta_v q_s$ scales similarly to $\overline{q_{sb}}$, and the circulation weakens rapidly with warming. Another factor is that Vecchi and Soden (2007) changed from a threshold of 0 Pa s^{-1}, which includes extratropical regions of ascending motion, to a threshold of 0.05 Pa s^{-1}, which limits the area considered to a few, strongly ascending tropical locations, while using global-mean precipitation and surface specific humidity in both cases. The utility of global-mean scaling estimates for local circulation changes is assessed in Figs. 5 and 6, which show that they do not generally account for the simulation results. Because changing the threshold changes both the geographic area under consideration and vertical structure, it is unclear which is more important.

REFERENCES

Back, L. E., and C. S. Bretherton, 2006: Geographic variability in the export of moist static energy and vertical motion profiles in the tropical Pacific. *Geophys. Res. Lett.,* **33,** L17810, doi:10.1029/2006GL026672.

Betts, A. K., 1998: Climate-convection feedbacks: Some further issues. *Climatic Change,* **39,** 35–38.

——, and W. L. Ridgway, 1989: Climatic equilibrium of the atmospheric convective boundary layer over a tropical ocean. *J. Atmos. Sci.,* **46,** 2621–2641.

Bordoni, S., 2007: On the role of eddies in monsoonal circulations: Observations and theory. Ph.D. thesis, University of California, Los Angeles, 195 pp.

——, and T. Schneider, 2008: Monsoons as eddy-mediated regime transitions of the tropical overturning circulation. *Nat. Geosci.,* **1,** 515–519.

Charney, J. G., 1963: A note on large-scale motions in the tropics. *J. Atmos. Sci.,* **20,** 607–609.

Clement, A. C., R. Seager, M. A. Cane, and S. E. Zebiak, 1996: An ocean dynamical thermostat. *J. Climate,* **9,** 2190–2196.

DiNezio, P. N., A. C. Clement, G. A. Vecchi, B. J. Soden, B. P. Kirtman, and S. K. Lee, 2009: Climate response of the equatorial Pacific to global warming. *J. Climate,* **22,** 4873–4892.

Fedorov, A. V., P. S. Dekens, M. McCarthy, A. C. Ravelo, P. B. DeMenocal, M. Barreiro, R. C. Pacanowski, and S. G. Philander, 2006: The Pliocene paradox (mechanisms for a permanent El Niño). *Science,* **312,** 1485–1489.

Frierson, D. M. W., 2007: The dynamics of idealized convection schemes and their effect on the zonally averaged tropical circulation. *J. Atmos. Sci.,* **64,** 1959–1976.

——, I. M. Held, and P. Zurita-Gotor, 2006: A gray-radiation aquaplanet moist GCM. Part I: Static stability and eddy scale. *J. Atmos. Sci.,* **63,** 2548–2566.

Hartmann, D. L., and K. Larson, 2002: An important constraint on tropical cloud-climate feedback. *Geophys. Res. Lett.,* **29,** 1951, doi:10.1029/2002GL015835.

Held, I. M., and B. J. Soden, 2006: Robust responses of the hydrological cycle to global warming. *J. Climate,* **19,** 5686–5699.

——, M. Winton, K. Takahashi, T. Delworth, F. Zeng, and G. K. Vallis, 2010: Probing the fast and slow components of global warming by returning abruptly to preindustrial forcing. *J. Climate,* **23,** 2418–2427.

Iribarne, J. V., and W. L. Godson, 1981: *Atmospheric Thermodynamics*. 2nd ed. *Geophys. Astrophys. Monogr.,* Vol. 6, D. Reidel, 259 pp.

Knutson, T. R., and S. Manabe, 1995: Time-mean response over the tropical Pacific to increased CO_2 in a coupled ocean–atmosphere model. *J. Climate,* **8,** 2181–2199.

Levine, X. J., and T. Schneider, 2011: Response of the Hadley circulation to climate change in an aquaplanet GCM coupled to a simple representation of ocean heat transport. *J. Atmos. Sci.,* **68,** 769–783.

Lindzen, R. S., and S. Nigam, 1987: On the role of sea surface temperature gradients in forcing low-level winds and convergence in the tropics. *J. Atmos. Sci.,* **44,** 2418–2436.

Meehl, G. A., and Coauthors, 2007: Global climate projections. *Climate Change 2007: The Physical Science Basis,* S. Solomon et al., Eds., Cambridge University Press, 747–845.

O'Gorman, P. A., and C. J. Muller, 2010: How closely do changes in surface and column water vapor follow Clausius–Clapeyron scaling in climate change simulations? *Environ. Res. Lett.,* **5,** 025207, doi:10.1088/1748-9326/5/2/025207.

——, and T. Schneider, 2008a: Energy of midlatitude transient eddies in idealized simulations of changed climates. *J. Climate,* **21,** 5797–5806.

——, and ——, 2008b: The hydrological cycle over a wide range of climates simulated with an idealized GCM. *J. Climate,* **21,** 3815–3832.

Peters, M. E., Z. Kuang, and C. C. Walker, 2008: Analysis of atmospheric energy transport in ERA-40 and implications for simple models of the mean tropical circulation. *J. Climate,* **21,** 5229–5241.

Pierrehumbert, R. T., 2010: *Principles of Planetary Climate*. Cambridge University Press, 688 pp.

Schneider, T., P. A. O'Gorman, and X. J. Levine, 2010: Water vapor and the dynamics of climate changes. *Rev. Geophys.,* **48,** RG3001, doi:10.1029/2009RG000302.

Sobel, A. H., 2007: Simple models of ensemble-averaged tropical precipitation and surface wind, given the sea surface temperature. *The Global Circulation of the Atmosphere,* T. Schneider and A. H. Sobel, Eds., Princeton University Press, 219–251.

——, J. Nilsson, and L. M. Polvani, 2001: The weak temperature gradient approximation and balanced tropical moisture waves. *J. Atmos. Sci.,* **58,** 3650–3665.

——, E. D. Maloney, G. Bellon, and D. M. Frierson, 2010: Surface fluxes and tropical intraseasonal variability: A reassessment. *J. Adv. Earth Model. Syst.,* **2,** 1–27.

Trenberth, K. E., J. M. Caron, and D. P. Stepaniak, 2001: The atmospheric energy budget and implications for surface fluxes and ocean heat transports. *Climate Dyn.,* **17,** 259–276.

Vecchi, G. A., and B. J. Soden, 2007: Global warming and the weakening of the tropical circulation. *J. Climate,* **20,** 4316–4340.

——, ——, A. T. Wittenberg, I. M. Held, A. Leetmaa, and M. J. Harrison, 2006: Weakening of tropical Pacific atmospheric circulation due to anthropogenic forcing. *Nature,* **441,** 73–76.

Wunsch, C., 2009: A perpetually running ENSO in the Pliocene? *J. Climate,* **22,** 3506–3510.

Xie, S.-P., C. Deser, G. A. Vecchi, J. Ma, H. Teng, and A. T. Wittenberg, 2010: Global warming pattern formation: Sea surface temperature and rainfall. *J. Climate,* **23,** 966–986.